N78-24053

EXTERNALLY BLOWN FLAP IMPINGEMENT PARAMETER

Danny R. Hoad
Langley Directorate, U.S. Army Air Mobility R&D Laboratory

SUMMARY

This paper presents a comparison of the performance of two externally blown flap (EBF) wind-tunnel models with an engine-exhaust flap impingement correlation parameter. One model was a four-engine EBF triple-slotted flap transport. Isolated engine wake surveys were conducted to define the wake properties of five separate engine configurations for which performance data were available. The other model was a two-engine EBF transport for which the engine wake properties were estimated. The correlation parameter was a function of engine-exhaust dynamic pressure at the flap location, area of engine-exhaust flap impingement, total exhaust area at the flap location, and engine thrust. The distribution of dynamic pressure for the first model was measured; however, the distribution for the second model was assumed to be uniform.

INTRODUCTION

Numerous concepts have been developed for achieving short-take-off-and-landing (STOL) performance. One approach which was selected for an advanced medium STOL transport (AMST) configuration, the YC-15, is the externally blown flap (EBF). Most EBF concept development has been achieved with experimental investigations (refs. 1 to 8) of various engine and airframe configurations. While very limited analyses (refs. 9 to 11) of these configurations have been attempted, some work has been done with an empirical analysis using a correlation parameter (impingement parameter) based on the vertical distance that the flap trailing edge extends into the jet exhaust from the engine center line and the radius of the jet exhaust at the flap trailing edge. (See ref. 12.)

The present paper describes the results of a relatively simple analysis based on an engine-exhaust flap impingement parameter, which is a function of the engine-exhaust dynamic pressure at the flap location, the area of engine-exhaust flap impingement, the total exhaust area at the flap location, and the thrust. Isolated engine wake surveys were conducted to define this parameter for one of the EBF models for which aerodynamic performance data were available (ref. 2). A uniform dynamic pressure profile was assumed to determine this parameter for the other EBF model. (See ref. 13.)

SYMBOLS

A_f total area of engine exhaust which impinges on flap, m^2

$A_{f,i}$ incremental area of engine exhaust which impinges on flap, m^2

A_j total area of engine exhaust at flap location, m^2

C_L lift coefficient, $\frac{\text{Lift}}{qS}$

$C_{L,tr}$ thrust-removed lift coefficient

C_μ thrust coefficient, $\frac{\text{Thrust}}{qS}$

c local wing chord, m

P_A engine-exhaust flap impingement parameter

q free-stream dynamic pressure, N/m^2

$q_{f,i}$ incremental dynamic pressure of engine exhaust which impinges on flap, N/m^2

q_j engine-exhaust dynamic pressure which impinges on flap, N/m^2

S wing area, m^2

T static thrust, N

z vertical distance, m

α angle of attack, deg

δ_f nominal flap deflection angle, deg

δ_j engine-exhaust deflection (measured from body axis), $\tan^{-1} \frac{\text{Normal force}}{\text{Axial force}}$, deg

η static-thrust recovery efficiency, $\frac{\sqrt{(\text{Normal force})^2 + (\text{Axial force})^2}}{T}$

Abbreviations:

BPR **bypass ratio**

EBF **externally blown flap**

MODELS

Two wind-tunnel investigations were conducted to determine the effect of different engine-exhaust characteristics on the performance of two separate EBF transport configurations (figs. 1 and 2).

A four-engine EBF transport (model 1, fig. 1) was tested in the Langley V/STOL tunnel. It had a 25° quarter-chord sweep, leading-edge slats deflected 50°, and triple-slotted full-span flaps whose elements were deflected 0°, 20°, and 40°, respectively, for the take-off configuration, and 15°, 35°, and 55°, respectively, for the landing configuration. The engines were simulated by a two-part ejector similar to that in figure 3. Each engine simulator was fitted with five separate cowl assemblies intended to represent five different engine configurations (fig. 4): (1) TF34 engine (BPR 6.2), (2) TF34 with noise suppressor nozzle (daisy nozzle), (3) stretched version of the TF34 (modified BPR 6.2), (4) JT15D engine (BPR 3.2), and (5) high-bypass-ratio engine (BPR 10). The modified BPR 6.2 engine was built so that the engine exit would be at the same chordwise location as the fan exit on the daisy nozzle. The BPR of these engine simulators does not describe in any way the size, horizontal position, or vertical position of the simulator, but is only intended to be a means of nomenclature. The important aspects of the simulator are not the characteristics at the exit, but the wake characteristics at the location of the flap as is evident subsequently in this paper. Since the exhaust and wake characteristics of the several full-scale engines represented are unknown, it is not possible to relate the present results to the performance of the full-scale engines. For further details of this model see reference 2.

A two-engine straight-wing EBF transport (model 2, fig. 2) was tested in the 5.18-m test section of the Langley 300-MPH 7- by 10-foot tunnel. It had a leading-edge slat deflected 40°, a double-slotted flap deflected 40° for the take-off configuration, and a triple-slotted flap deflected 60° for the landing configuration. The engines were simulated by a two-part ejector as presented in figure 5. The engine vertical position on this configuration was varied (to three positions) to determine its effect on the performance of the configuration (fig. 6).

TEST

Both models were mounted on a sting-supported six-component strain-gage balance for measurements of the total forces and moments. Isolated engine wake surveys were conducted for each engine configuration on model 1 so that the engine-exhaust flap impingement parameter could be determined. Dynamic pressure measurements were made with a pressure rake positioned so that the probes were alined along a radial line from the geometric center line. Four radial positions were chosen for the daisy nozzle and two radial positions were chosen for the other four engine simulators. These measurements were repeated at various downstream locations to obtain dynamic pressure profile characteristics. Isolated engine wake surveys were not available for the engine simulators on model 2. Since the same engine was used in all three positions, it was felt that assuming a 10° spread angle would be sufficient to determine the relative influence of the exhaust flap impingement parameter.

Jet deflection angles δ_j and static-thrust recovery efficiency η for both models were determined from measurements of the normal and axial forces made in the static-thrust condition with flaps deflected and leading-edge slat deployed.

CALCULATIONS

Isolated engine wake surveys were available for each engine configuration used on model 1. The flap impingement parameter was computed using the distribution of dynamic pressure at the flap location in the following manner:

$$P_A = \left(\sum_i q_{f,i} A_{f,i}\right) \frac{S}{TA_j} \sin \delta_f \qquad (1)$$

A schematic of exhaust impingement on the flap is presented in figure 7. The term $\sum_i q_{f,i} A_{f,i}$ can be seen as a summation of all the dynamic pressure measurements multiplied by the associated flap area on which they impinge In equation (1), A_j is the total area of engine exhaust at the flap impingement plane and δ_f is the nominal flap deflection angle. Since the term $\sum_i q_{f,i} A_{f,i}$ is a thrust or force term, the parameter was divided by thrust T and nondimensionalized by an arbitrary constant S (wing area).

Since isolated engine wake surveys were not available for the engine configuration used on model 2, the dynamic pressure was assumed to be uniform at the flap location. The exhaust was assumed to spread at an angle of 10° to determine the area of the exhaust at the flap location. The impingement

parameter in this case is slightly simplified in that the dynamic pressure is assumed constant over the flap; that is,

$$P_A = q_j A_f \frac{S}{TA_j} \sin \delta_f \tag{2}$$

The lift developed by a powered-lift system can be separated into three parts according to source: (1) the lift that would have been produced by the unpowered wing, (2) the lift due to the component of the jet which has been redirected by the flap system, and (3) the lift due to circulation induced by the blowing. If the portion of the lift due to the jet is removed from the total lift, a thrust-removed lift coefficient given by

$$C_{L,tr} = C_L - \eta C_\mu \sin (\delta_j + \alpha) \tag{3}$$

remains which can be related to the flap impingement parameter.

RESULTS AND DISCUSSION

The flap static turning effectiveness parameters for both models are presented in figure 8 in polar coordinate form. These parameters for the five engine simulators on model 1 and the three positions of the engine simulator on model 2 in the take-off and landing configurations are presented at a particular level of thrust. This was the thrust level used to obtain a thrust coefficient of 2 in the wind-tunnel test for each configuration.

The perpendicular distance from a data point in figure 8 to the horizontal axis would represent the lift component due to thrust at an angle of attack of 0°. If it were assumed that with zero power all engine simulator configurations had identical characteristics and that the only additions to the aerodynamic characteristics at an angle of attack of 0° were those components in figure 8, an assessment could be made as to the relative merit of the configurations. As discussed in reference 2, this assessment of the aerodynamic characteristics of an engine model configuration is not necessarily true. A more pertinent comparison based on the engine-exhaust flap impingement parameter is presented in this paper.

The flap impingement parameter is a correlation parameter which relates the engine-exhaust properties to the performance of the engine model configuration. The lift coefficient performance and impingement parameter are presented for several model flap combinations at an angle of attack of 0° as follows:

Figure	Model	Flap configuration
9	1	Landing
10	1	Take-off
11	2	Landing
12	2	Take-off

The effect of engine configuration for landing flap deflection on model 1 (fig. 9) indicates that the engine simulators which produce the largest impingement parameter (BPR 6.2 and modified BPR 6.2) provide the largest lift coefficient. The simulator which produces the smallest impingement parameter (BPR 3.2) provides the smallest lift coefficient. This impingement parameter is really a measure of the proportion of $q_j A_j$, or momentum, which impinges on the flap and, in turn, is deflected and induces circulation. This would indicate that the more momentum captured by the flap system, the better the combination will perform. The effect of engine configuration for take-off flap deflection on model 1 (fig. 10) is similar except for the relative performance and magnitude of impingement parameter for the daisy nozzle. The daisy nozzle has eight fan lobes and nine gas generator lobes. Since the wake survey for this engine included only two fan lobes and two gas generator lobes, it was not comprehensive enough to adequately define the profile.

The comparisons of performance and impingement parameter for model 2 with landing and take-off flap deflections are presented in figures 11 and 12. The results for the landing configuration indicate that moving the engine exhaust vertically toward the wing lower surface increases the proportion of $q_j A_j$, or momentum, which is captured by the flap system and, in turn, generates increased lift. Figure 12 for the take-off configuration indicates the same trend, although at a somewhat lower value because there is less flap projection to capture the exhaust.

To further relate this flap impingement parameter to the lift performance of the models, the thrust-removed lift coefficient at an angle of attack of 0° was computed for each configuration and is presented in figure 13 as a function of the impingement parameter. It is evident that the thrust-removed lift coefficient is the prime aerodynamic factor which can be related to the impingement parameter, because the data fit a straight line which intercepts $P_A = 0$ at the value of C_L which corresponds to the power-off condition. (In this case, P_A should be zero.) If the blowing did not induce supercirculation lift, these data points would be on horizontal lines. In each model, it can be seen that the landing configuration data describe a line with a larger slope than that for the take-off configuration. This is more evidence that since the landing flaps capture more of the exhaust flow, more circulation lift is induced. This again emphasizes the fact that the engine-exhaust flap impingement parameter is a measure of the proportion of momentum captured by the flap and provides a method to assess the relative performance of engine-wing combinations.

CONCLUDING REMARKS

This paper provides a technique to assess the relative performance of externally blown flap (EBF) configurations by means of an engine-exhaust flap impingement parameter. This parameter was determined to be a function of the proportion of momentum which is captured by the flap system.

The lift produced by an EBF configuration can be related to the proportion of momentum captured by the flap system. Furthermore, it has been shown that the thrust-removed lift coefficient can be directly related to this captured momentum, defined by the engine-exhaust flap impingement parameter.

REFERENCES

1. STOL Technology. NASA SP 320, 1972.

2. Hoad, Danny R.: Longitudinal Aerodynamic Characteristics of an Externally Blown Flap Powered-Lift Model With Several Propulsive System Simulators. NASA TN D-7670, 1974.

3. Parlett, Lysle P.; Freeman, Delma C., Jr.; and Smith, Charles C., Jr.: Wind-Tunnel Investigation of a Jet Transport Airplane Configuration With High Thrust-Weight Ratio and an External-Flow Jet Flap. NASA TN D-6058, 1970.

4. Smith, Charles C., Jr.: Effect of Wing Aspect Ratio and Flap Span on Aerodynamic Characteristics of an Externally Blown Jet-Flap STOL Model. NASA TN D-7205, 1973.

5. Parlett, Lysle P.; Smith, Charles C., Jr.; and Megrail, James L.: Wind-Tunnel Investigation of Effects of Variations in Reynolds Number and Leading-Edge Treatment on the Aerodynamic Characteristics of an Externally Blown Jet-Flap Configuration. NASA TN D-7194, 1973.

6. Aoyagi, Kiyoshi; Falarski, Michael D.; and Koenig, David G.: Wind-Tunnel Investigation of a Large-Scale 25° Swept-Wing Jet Transport Model With an External Blowing Triple-Slotted Flap. NASA TM X-62197, 1973.

7. Freeman, Delma C., Jr.; Parlett, Lysle P.; and Henderson, Robert L.: Wind-Tunnel Investigation of a Jet Transport Airplane Configuration With an External-Flow Jet Flap and Inboard Pod-Mounted Engines. NASA TN D-7004, 1970.

8. Vogler, Raymond D.: Wind-Tunnel Investigation of a Four-Engine Externally Blowing Jet-Flap STOL Airplane Model. NASA TN D-7034, 1970.

9. Johnson, William G., Jr.; and Kardas, Gerald E.: A Wind-Tunnel Investigation of the Wake Near the Trailing Edge of a Deflected Externally Blown Flap. NASA TM X-3079, 1974.

10. Goldhammer, M. I.; Lopez, M. L.; and Shen, C. C.: Methods for Predicting the Aerodynamic and Stability and Control Characteristics of STOL Aircraft. Volume I - Basic Theoretical Methods. AFFDL-TR-73-146-Vol. I, U.S. Air Force, Dec. 1973.

11. May, Fred; and Widdicon, Colin A.: STOL High-Lift Design Study. Volume 1. State-of-the-Art Review of STOL Aerodynamic Technology. AFFDL-TR-71-26-Vol. I, U.S. Air Force, Apr. 1971.

12. Roe, M. H.; Renselaer, D. J.; Quam, R. A.; et al.: STOL Tactical Aircraft Investigation - Externally Blown Flap. Volume II - Design Compendium. AFFDL-TR-73-20, Vol. II, U.S. Air Force, Apr. 1973. (Available from DDC as AD 770 110.)

13. Johnson, William G., Jr.: Longitudinal Aerodynamic Characteristics of a Wing-Body Combination Having a Rectangular, Aspect-Ratio-6, Slotted Supercritical Wing With Externally Blown Flaps. NASA TM X-2388, 1971.

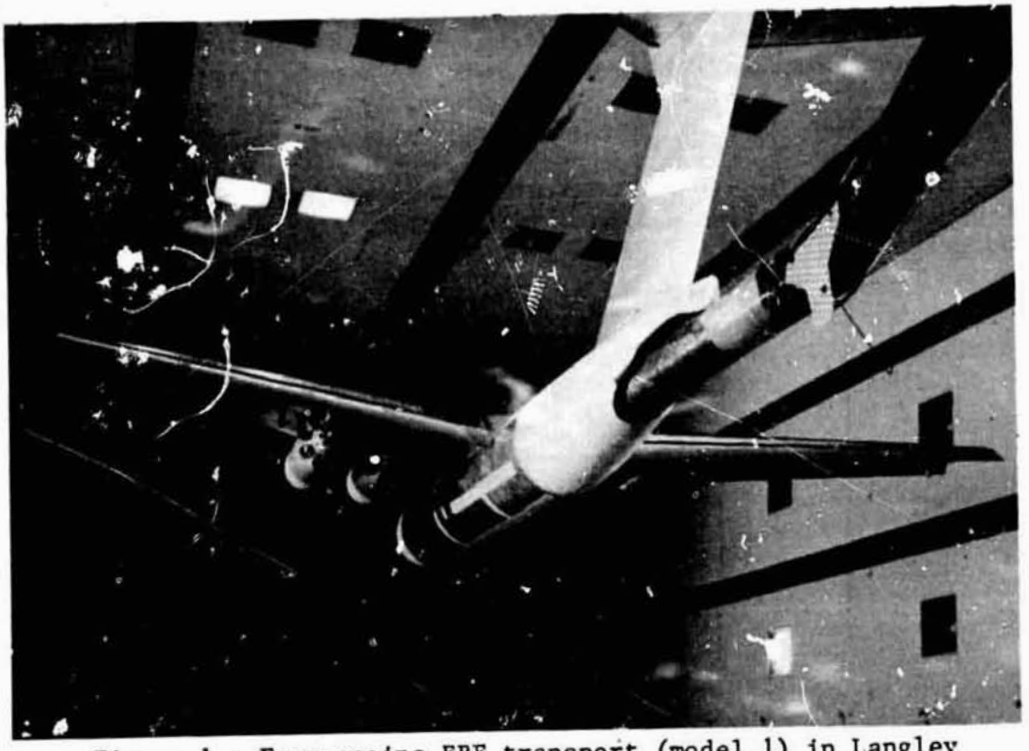

Figure 1.- Four-engine EBF transport (model 1) in Langley V/STOL tunnel.

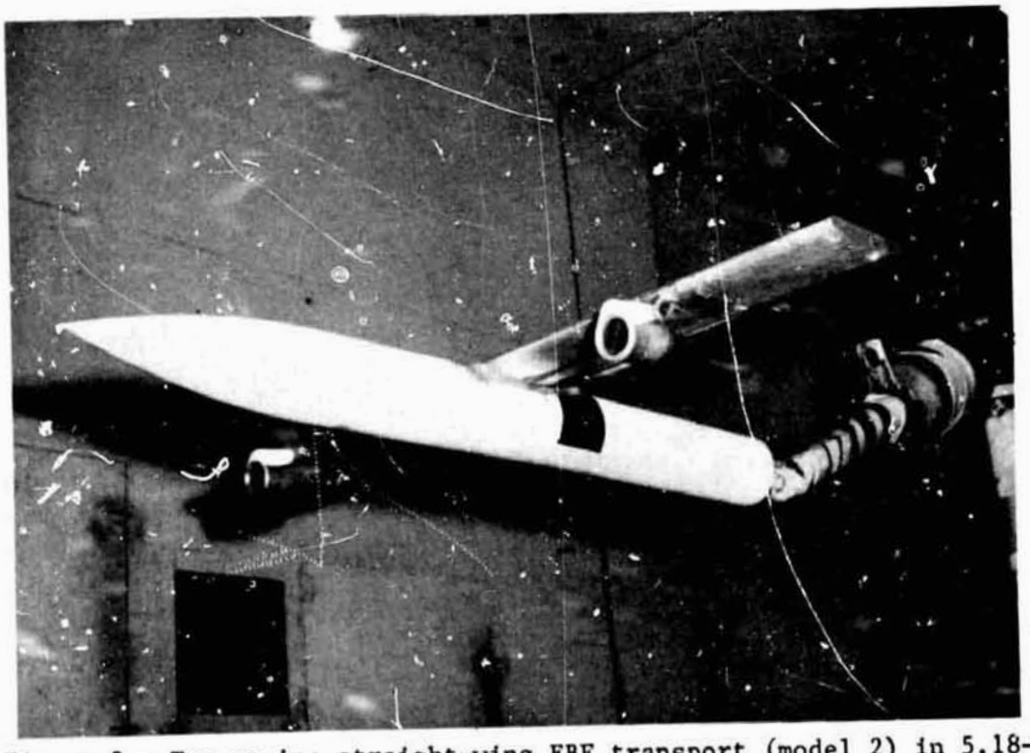

Figure 2.- Two-engine straight-wing EBF transport (model 2) in 5.18-m test section of Langley 300-MPH 7- by 10-foot tunnel.

ORIGINAL PAGE IS
OF POOR QUALITY

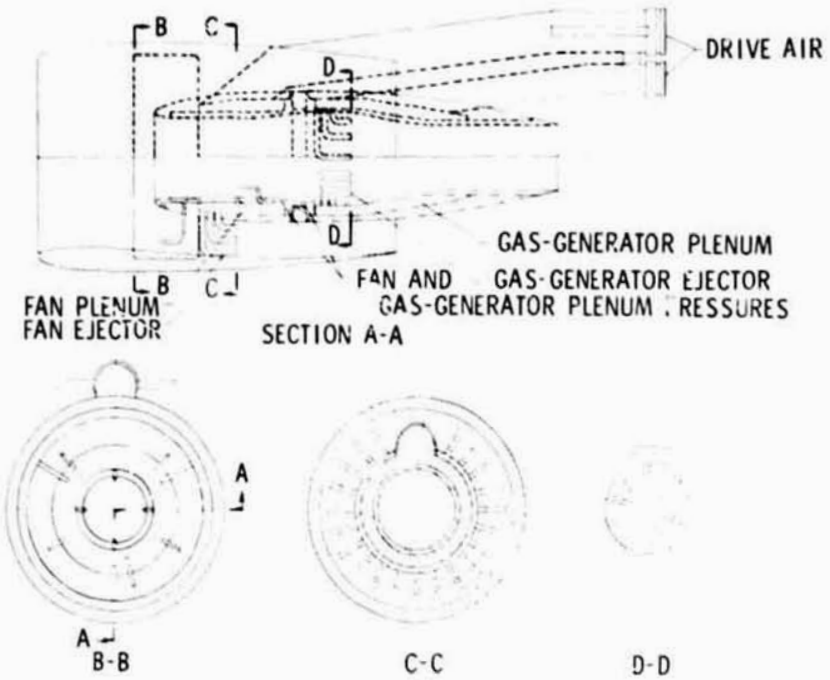

Figure 3.- Two-part engine simulator for model 1.

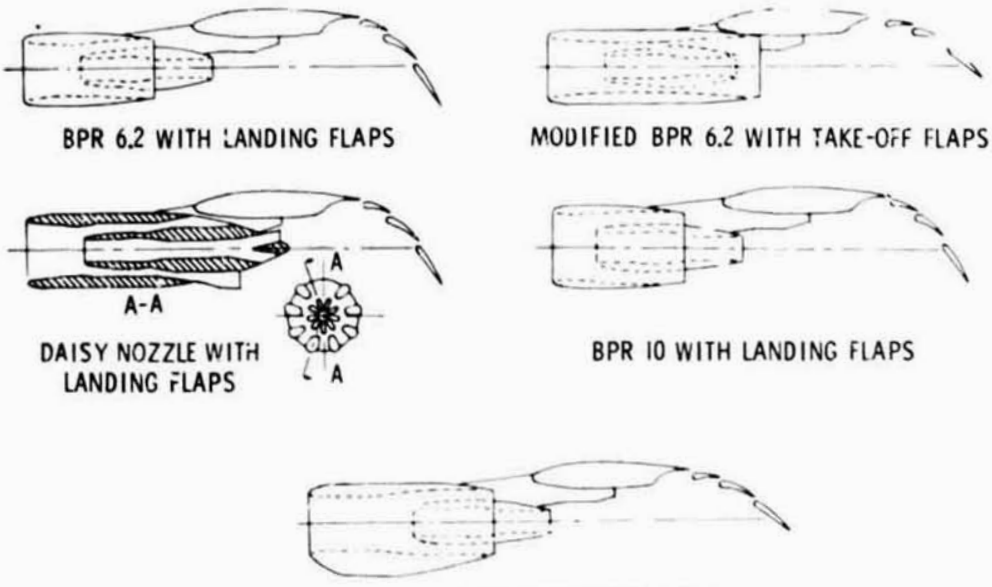

Figure 4.- Engine configurations used on model 1.

REPRODUCIBILITY OF THE
ORIGINAL PAGE IS POOR

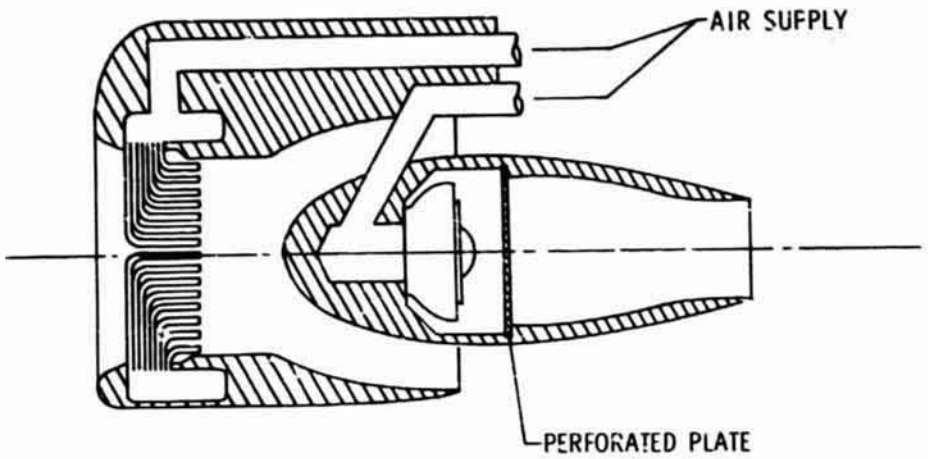

Figure 5.- Two-part engine simulator for model 2.

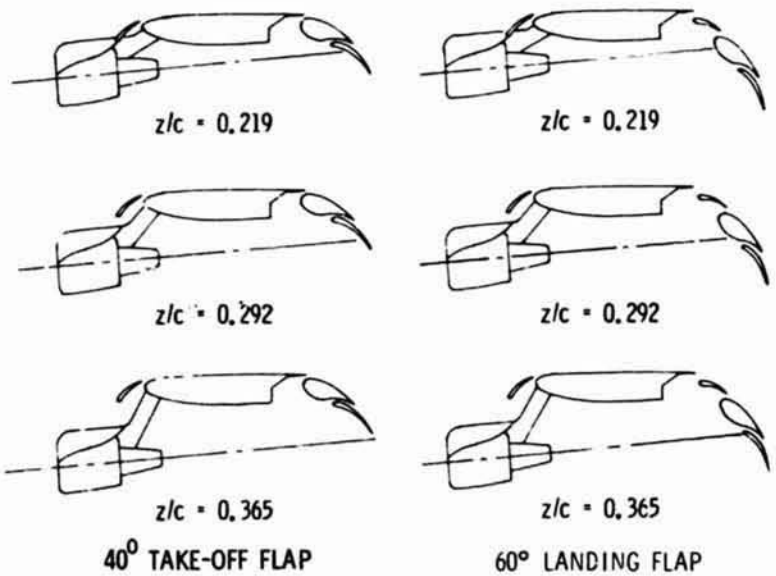

Figure 6.- Engine positions used on model 2.

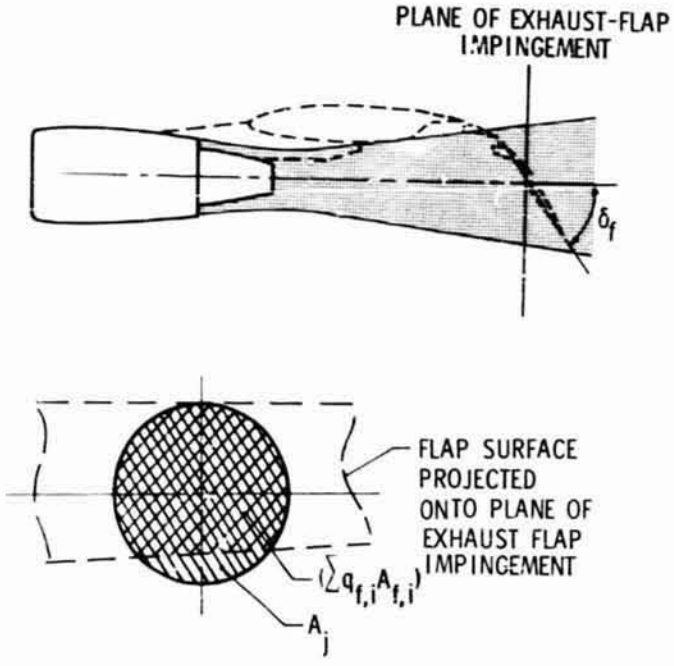

Figure 7.- Schematic of exhaust flap impingement.

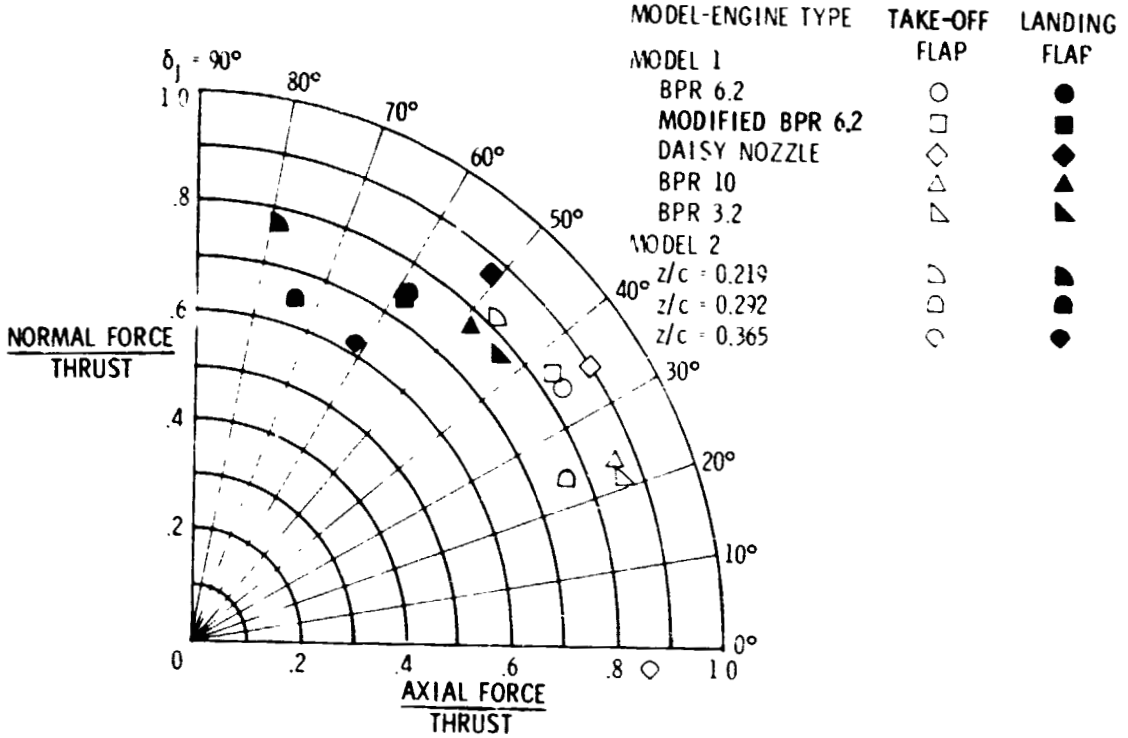

Figure 8.- Flap static turning effectiveness for models 1 and 2.

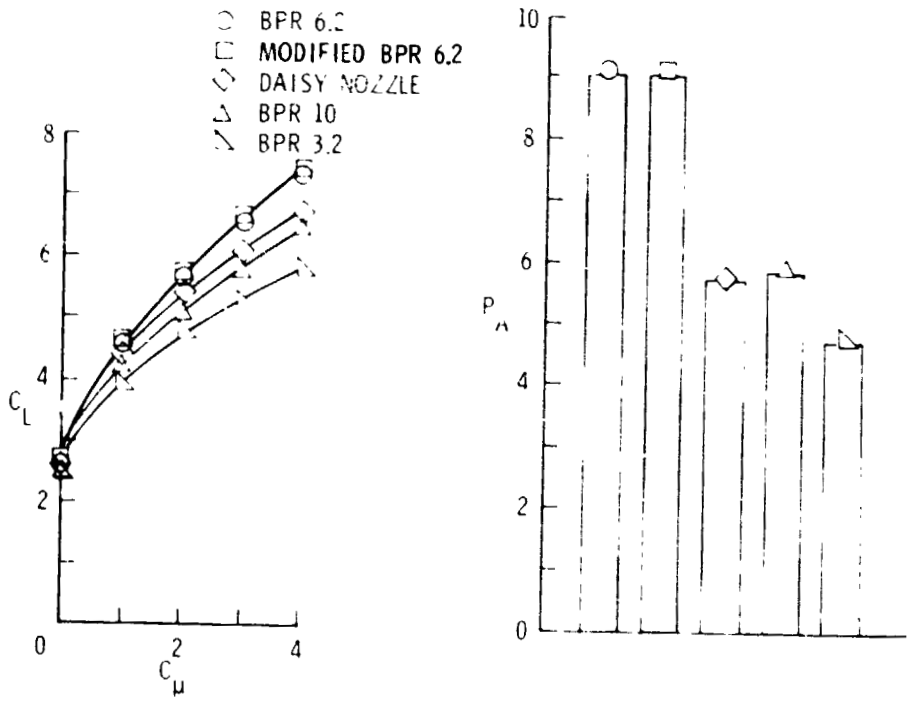

Figure 9.- Performance and impingement parameter for model 1 with landing flap deflection. $\alpha = 0°$.

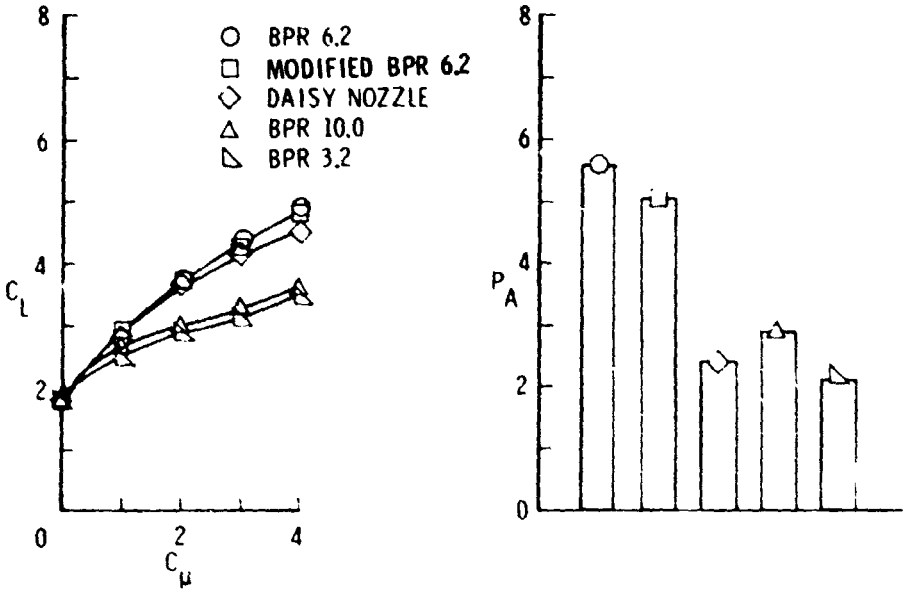

Figure 10.- Performance and impingement parameter for model 1 with take-off flap deflection. $\alpha = 0^\circ$.

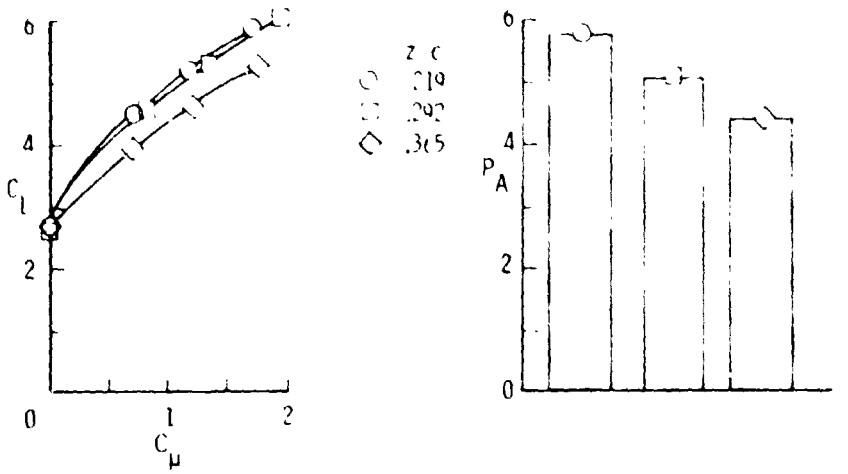

Figure 11.- Performance and impingement parameter for model 2 with landing flap deflection. $\alpha = 0^\circ$.

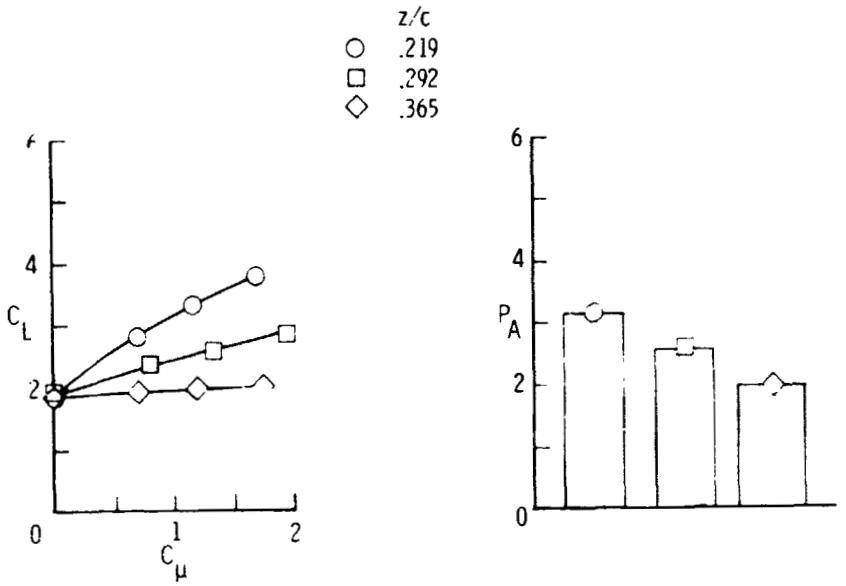

Figure 12.- Performance and impingement parameter for model 2 with take-off flap deflection. $\alpha = 0^o$.

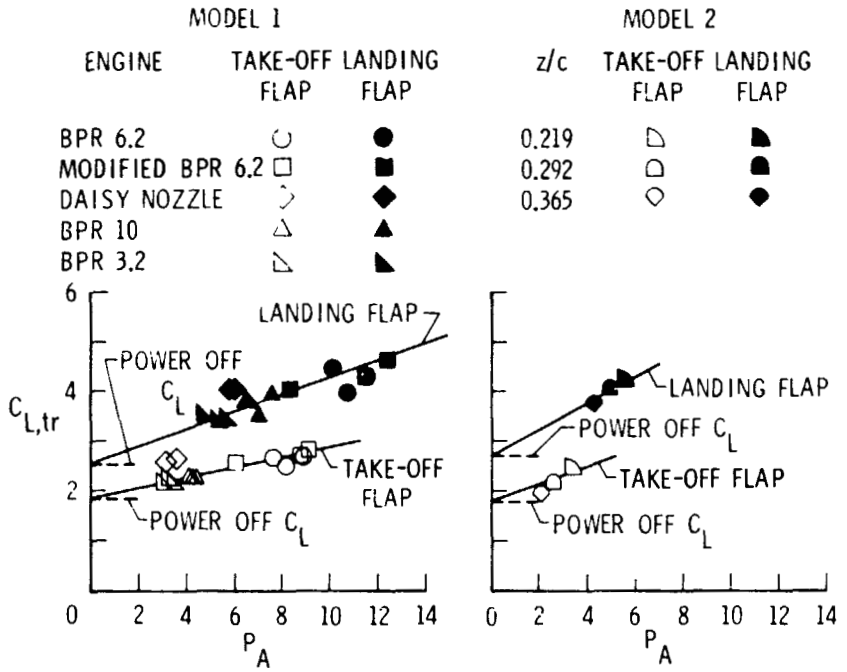

Figure 13.- Thrust-removed lift coefficient as a function of impingement parameter. $\alpha = 0^o$.